ARL-RP-0537 ● SEP 2015

US Army Research Laboratory

Raman Detection of Improvised Explosive Device (IED) Material Fabricated Using Drop-on-Demand Inkjet Technology on Several Real World Surfaces

by Mikella E Farrell, Ellen L Holthoff, and Paul M Pellegrino

A reprint from Proc. of SPIE Vol. 9454 94540T-1.

Approved for public release; distribution unlimited.

NOTICES

Disclaimers

The findings in this report are not to be construed as an official Department of the Army position unless so designated by other authorized documents.

Citation of manufacturer's or trade names does not constitute an official endorsement or approval of the use thereof.

Destroy this report when it is no longer needed. Do not return it to the originator.

ARL-RP-0537 ● SEP 2015

US Army Research Laboratory

Raman Detection of Improvised Explosive Device (IED) Material Fabricated Using Drop-on-Demand Inkjet Technology on Several Real World Surfaces

by Mikella E Farrell, Ellen L Holthoff, and Paul M Pellegrino
Sensors and Electron Devices Directorate, ARL

A reprint from Proc. of SPIE Vol. 9454 94540T-1.

Approved for public release; distribution unlimited.

REPORT DOCUMENTATION PAGE

Form Approved
OMB No. 0704-0188

Public reporting burden for this collection of information is estimated to average 1 hour per response, including the time for reviewing instructions, searching existing data sources, gathering and maintaining the data needed, and completing and reviewing the collection information. Send comments regarding this burden estimate or any other aspect of this collection of information, including suggestions for reducing the burden, to Department of Defense, Washington Headquarters Services, Directorate for Information Operations and Reports (0704-0188), 1215 Jefferson Davis Highway, Suite 1204, Arlington, VA 22202-4302. Respondents should be aware that notwithstanding any other provision of law, no person shall be subject to any penalty for failing to comply with a collection of information if it does not display a currently valid OMB control number.
PLEASE DO NOT RETURN YOUR FORM TO THE ABOVE ADDRESS.

1. REPORT DATE *(DD-MM-YYYY)*	2. REPORT TYPE	3. DATES COVERED (From - To)
Sep 2015	Reprint	

4. TITLE AND SUBTITLE
Raman Detection of Improvised Explosive Device (IED) Material Fabricated Using Drop-on-Demand Inkjet Technology on Several Real World Surfaces

5a. CONTRACT NUMBER

5b. GRANT NUMBER

5c. PROGRAM ELEMENT NUMBER

6. AUTHOR(S)
Mikella E Farrell, Ellen L. Holthoff, and Paul M Pellegrino

5d. PROJECT NUMBER

5e. TASK NUMBER

5f. WORK UNIT NUMBER

7. PERFORMING ORGANIZATION NAME(S) AND ADDRESS(ES)
US Army Research Laboratory
ATTN: RDRL-SEE-E
2800 Powder Mill Road
Adelphi, MD 20783-1138

8. PERFORMING ORGANIZATION REPORT NUMBER
ARL-RP-0537

9. SPONSORING/MONITORING AGENCY NAME(S) AND ADDRESS(ES)

10. SPONSOR/MONITOR'S ACRONYM(S)

11. SPONSOR/MONITOR'S REPORT NUMBER(S)

12. DISTRIBUTION/AVAILABILITY STATEMENT
Approved for public release; distribution unlimited.

13. SUPPLEMENTARY NOTES
A reprint from Proc. of SPIE Vol. 9454 94540T-1.

14. ABSTRACT
The requirement to detect hazardous materials (i.e., chemical, biological, and explosive) on a host of materials has led to the development of hazard detection systems. These new technologies and their capabilities could have immediate uses for the US military, national security agencies, and environmental response teams in efforts to keep people secure and safe. In particular, due to the increasing use by terrorists, the detection of common explosives and improvised explosive device (IED) materials have motivated research efforts toward detecting trace (i.e., particle level) quantities on multiple commonly encountered surfaces (e.g., textiles, metals, plastics, natural products, and even people). Non-destructive detection techniques can detect trace quantities of explosive materials; however, it can be challenging in the presence of a complex chemical background. One spectroscopic technique gaining increased attention for detection is Raman.
One popular explosive precursor material is ammonium nitrate (AN). The material AN has many agricultural applications, however it can also be used in the fabrication of IEDs or homemade explosives (HMEs). In this paper, known amounts of AN will be deposited using an inkjet printer into several different common material surfaces (e.g., wood, human hair, textiles, metals, plastics). The materials are characterized with microscope images and by collecting Raman spectral data. In this report the detection and identification of AN will be demonstrated.

15. SUBJECT TERMS
Raman, substrate, Ammonium nitrate, plastic, fabric, human hair, wood, rubber

16. SECURITY CLASSIFICATION OF:			17. LIMITATION OF ABSTRACT	18. NUMBER OF PAGES	19a. NAME OF RESPONSIBLE PERSON
a. REPORT	b. ABSTRACT	c. THIS PAGE			Mikella E Farrell
Unclassified	Unclassified	Unclassified	UU	18	19b. TELEPHONE NUMBER (Include area code) 301-394-0948

Standard Form 298 (Rev. 8/98)
Prescribed by ANSI Std. Z39.18

Raman Detection of improvised explosive device (IED) material fabricated using drop-on-demand Inkjet Technology on several real world surfaces

Mikella E. Farrell, Ellen L. Holthoff and Paul M. Pellegrino
U.S. Army Research Labs, RDRL-SEE-E, 2800 Powder Mill Rd., Adelphi, MD 21228

ABSTRACT

The requirement to detect hazardous materials (i.e., chemical, biological, and explosive) on a host of materials has led to the development of hazard detection systems. These new technologies and their capabilities could have immediate uses for the US military, national security agencies, and environmental response teams in efforts to keep people secure and safe. In particular, due to the increasing use by terrorists, the detection of common explosives and improvised explosive device (IED) materials have motivated research efforts toward detecting trace (i.e., particle level) quantities on multiple commonly encountered surfaces (e.g., textiles, metals, plastics, natural products, and even people). Non-destructive detection techniques can detect trace quantities of explosive materials; however, it can be challenging in the presence of a complex chemical background. One spectroscopic technique gaining increased attention for detection is Raman.

One popular explosive precursor material is ammonium nitrate (AN). The material AN has many agricultural applications, however it can also be used in the fabrication of IEDs or homemade explosives (HMEs). In this paper, known amounts of AN will be deposited using an inkjet printer into several different common material surfaces (e.g., wood, human hair, textiles, metals, plastics). The materials are characterized with microscope images and by collecting Raman spectral data. In this report the detection and identification of AN will be demonstrated.

Keywords: Raman, substrate, Ammonium nitrate, plastic, fabric, human hair, wood, rubber

1. INTRODUCTION

The requirement to detect hazardous materials has led to the development of hazard detection systems with immediate application to the US military, national security agencies, and environmental response teams. In particular, it has been demonstrated that the detection of common explosives and improvised explosive device (IED) substance particles on a host of materials including natural and manmade textiles, metals, and plastics; and naturally occurring materials like wood, stone, hair, or even skin can be an indicator of either suspicious objects or subjects. There are some standard techniques used for the detection of trace quantities of explosive materials. Some of these techniques for explosive material detection include gas chromatography[1], [2-4], x-ray analysis[5, 6], neutron activation [7-11], chemiluminescence[12-17], vapor detection via cantilever[18-21] systems and even biological techniques like dog noses[18-26] or honeybees[27, 28]. However, despite the vast array of available techniques, none of these have yet proven 100% effective and ruggedized in the presence of a complex chemical background and under standard theatre environments encountered.[29-39] Additionally, several of these techniques require significant sample preparation, and/or destruction to the samples. An alternative technique that does not require sample preparation or destruction is Raman or Raman-based spectroscopy[40-44].

One of many spectroscopic techniques gaining increased attention for the detection of hazard materials, Raman has generated significant interest[45-47]. The unique chemical "fingerprint" provided by Raman techniques allow for chemical identification within a complex environment. Additionally this is a technique that can apply to both standoff detection and bench top forensic hazard investigations. Raman spectroscopy[31, 34-38, 41, 48-57] is a detection technique generally used to measure the vibrational, rotational and low frequency modes in a system. Generally the interrogation light used is a monochromatic source like a laser. The laser light interacts with the molecule resulting in a frequency shift (increase or decrease) relative to the energy of the vibrating molecules. Advantages of using Raman-based detection techniques are that little to no sample preparation is necessary, there is little to no sample degradation, only a small quantity of material is needed, several different laser sources can be used, the technique is fairly insensitive to environmental conditions (like

Detection and Sensing of Mines, Explosive Objects, and Obscured Targets XX,
edited by Steven S. Bishop, Jason C. Isaacs, Proc. of SPIE Vol. 9454, 94540T
© 2015 SPIE · CCC code: 0277-786X/15/$18 · doi: 10.1117/12.2176553

Downloaded From: http://proceedings.spiedigitallibrary.org/ on 08/24/2015 Terms of Use: http://spiedigitallibrary.org/ss/TermsOfUse.aspx

water interference), and it can generate a "fingerprint" spectrum from which sample identification and quantification is possible. With all of these advantages, Raman has been shown to be a reliable means of Army and first responder relevant hazard detection with paramount features including preservation of samples for additional forensic testing.[58, 59]

There are many examples of hazardous materials encountered by the US military and first responders. Some examples of common explosives include octogen (HMX), 1,3,5-trinitroperhydro-1,3,5-triazine (RDX), 2,4,6-trinitrotoluene (TNT), and black powder. Common examples of IED/ homemade explosive (HME) components can include ammonium nitrate (AN) and urea. Many of these materials have well known Raman signatures that can be used for stand-off detection and identification. Some of these materials are also known to exist in multiple polymorphic phases[60-74] that can in part be attributed to concentration levels of material present, handling and storage methods used, and in some certain cases even the surface onto which the material has been deposited. Generally in fingerprint samples[75-83], explosive material particle sizes range from 10 µm to several hundred µms; with the bulk of the sample consisting of smaller sized particles. To validate the ability to measure these small particles, it is necessary to use a standardized deposition technique (i.e., inkjet printing) that can deliver known particle masses and particle sizes.

Inkjet printing[69, 84-86] is increasingly being used as a standardized means to create samples for the training and evaluation of hazard detection systems. Using an inkjet printer system, the user is able to deposit material (ranging from trace (<100 µg/cm^2) to bulk (> 100 µg/cm^2)) in specific locations, and deposit known volumes to each of those locations. Inkjet printing technologies have in part replaced some other means of coupon sample fabrication like drop and dry methods because they are more reliable, accurate and reproducible. Inkjet printed samples can be fabricated on several different substrate surfaces, including natural and manmade materials.

For this paper we demonstrate that inkjet technologies can be used to deposit material on a host of substrate types, and Raman spectroscopy can be employed for the successful detection and identification of the commonly used IED material, AN, on these substrates. The material AN was selected because it is a common fertilizer component that is useful in agricultural and industrial applications, and the production of HMEs and IEDs.[33, 39, 60-63, 65, 67, 87-99] Ammonium nitrate in pure format is generally described as a white crystalline material at standard temperature and humidity. AN has been previously shown to exist in at least five different crystal phases.[64] When phase transitions for AN are observed with Raman, the bands typically associated with symmetric stretch mode of NO_3^- [39, 100] shift from phase II at 1050 cm^{-1}, phase III at 1048 cm^{-1}, and phase IV at 1044 cm^{-1}. In previous printing and characterization efforts, we have observed that on a metal SERS substrates, it is possible to measure different phases of AN (concentration dependent). In an effort to characterize the nature of AN as it deposits on various object surfaces, AN was inkjet printed onto several common materials at both a bulk (>100 µg/cm^2) and trace (<100 µg/cm^2) concentrations. In this proceedings paper, Raman spectral information from the various concentrations of AN as deposited onto differing substrates including silicon, aluminum, polyethylene, various cloth materials, and human hair substrates is reported. It is the intent of this report to demonstrate the Raman detection capabilities and challenges on these various surfaces, and determine if various polymorphs can be observed.

2. EXPERIMENTAL

2.1. Reagents and Materials.

AN, methanol (MeOH), ethanol (EtOH), and distilled water were obtained from Sigma-Aldrich. All AN inkjet solutions were prepared at various concentrations in solvents of water, methanol or a mixture of these solvents. All solvents used were HPLC grade. All chemicals were used as received unless otherwise noted.

2.2. Printed Material Substrates.

Velveteen squares were procured from ScienceWare (catalog # 37848-001, off white tan) and were used as received.Poljean Cloth samples were procured from TedPella (catalog 381224, white matte finish) and used as received. Hair samples were procured from Hair imports (Gendale, NY). The hair material (Uzbecki brown hair) was used as received. The tarp sample was VWR and is described as top tarp white. Squares of material were cut from the larger sample. Samples were used as received. The polyethylene (PE) sample was cute from a larger sheet material. The silicon (Si) sample was cut from a larger Si wafer in house. Used as received without additional cleaning. Aluminium

Downloaded From: http://proceedings.spiedigitallibrary.org/ on 08/24/2015 Terms of Use: http://spiedigitallibrary.org/ss/TermsOfUse.aspx

samples were purchased from www.onlinesheetmetal.com. Samples were cut to 1 inch squares and were gently wiped clean with ethanol prior to use.

2.3. Instrumentation

Scanning electron microscope (SEM) images was obtained using a FEI environmental SEM (Quanta 200 FEG).

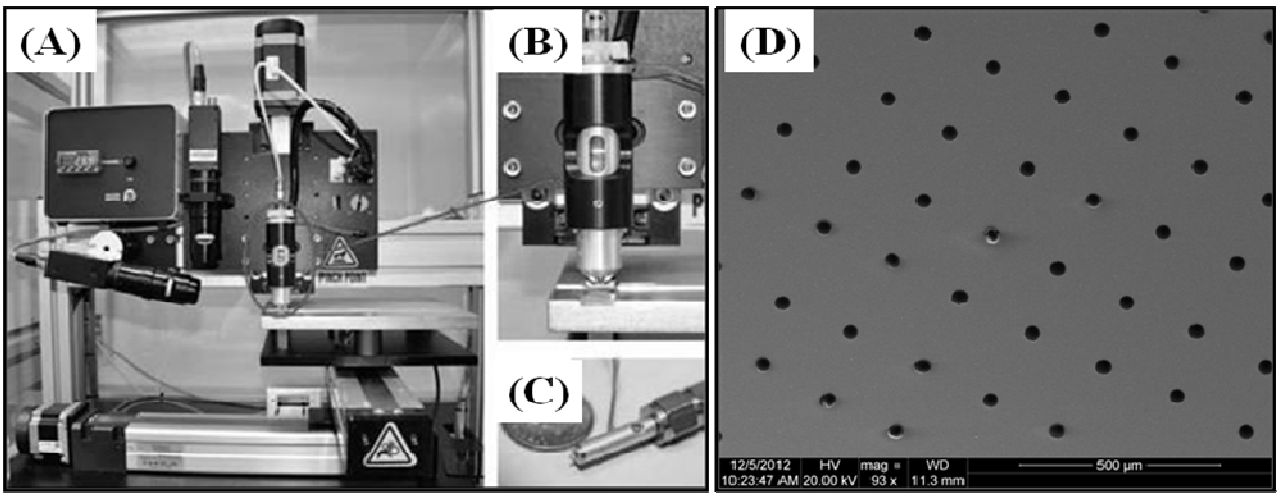

Figure. 2. Photographs of (A) JetLab 4 drop-on-demand inkjet printing platform; (B) dispensing device and ink solution encasement; and (C) print head assembly. In (D) SEM image of a printed AN sample demonstrating clear, distinct, uniform rows of printed materials.

Materials were produced using a JetLab® 4 (MicroFab Technologies) tabletop printing platform and have been previously documented.[101] Briefly, the JetLab® 4 is a drop-on-demand inkjet printing system with drop ejection drive electronics (JetDrive™ III), pressure control, a drop visualization system, and precision *X*, *Y*, *Z* motion control. The dispensing device (print head assembly, MJ-AL-01-060) consists of a glass capillary tube, with a 60 µm diameter orifice coupled to a piezoelectric element. Voltage pulses (20–25 V; rise time 1 µs; dwell time 28–32 µs; fall time 1 µs) applied to the piezo result in pressure fluctuations around the capillary. These pressure oscillations propagate through the printing fluid in the tube, resulting in ejection of a microdrop. Drops are visualized using synchronized strobe illumination and a charged coupled device (CCD) camera. Determining optimal jetting parameters is a trial-and-error process. Stable droplet ejection is achieved by visually observing expelled microdrops and adjusting voltage pulse parameters and capillary fluid backfill pressure. Conditions that provide the highest drop velocity without satellite droplet formation are desired. Printing was performed at a frequency of 250 Hz with a droplet velocity of ~2 m/s. Drop diameter was estimated to be ~60 µm, based on the capillary orifice diameter. During printing, a single substrate was placed on the sample stage. The print head remained fixed at a specified height while the stage moved to print a specified pattern. A rectangular array, which covers a rectangular area with rows of equidistant points, was pre-programmed based on the substrate size and desired sample concentration. An array pattern was chosen for the purpose of creating the effect of a homogeneous coating for optical interrogation. Depending on the desired concentration per unit area (e.g., $\mu g/cm^2$), the total number of drops needed to achieve the desired concentration in that area was calculated based on the mass of a single microdrop. Based on the number of total drops needed, the array spacing and drops needed per line can be calculated. These values are easily adjusted depending on concentration. Arrays were printed using the print on-the-fly mode. In this mode, the stage moves continuously as a single microdrop is dispensed at each array element. Print on-the-fly mode improves sample throughput. Concentrations of deposited materials have been validated using a secondary UV-Vis measurement. This method has been previously documented, and typically has R^2 values above 0.998 and RSDs of <3% or better. [32, 101]

Downloaded From: http://proceedings.spiedigitallibrary.org/ on 08/24/2015 Terms of Use: http://spiedigitallibrary.org/ss/TermsOfUse.aspx

2.4. Raman Measurements.

Raman data was recorded using a Renishaw inVia Reflex Raman microscope equipped with a near-infrared diode laser excitation source (λ = 785 nm). The light from the diode was focused onto the samples at the microscope stage through a 5X objective. A 5X or 20X objective was used for all measurements unless otherwise noted. Dispersion and resolution of the Renishaw vary with wavelength, but are typically 1 cm^{-1}, decreasing to 0.5 cm^{-1} for certain gratings and wavelengths. Prior to coupling into the microscope, the diode laser beam was circularized by inserting a pinhole into the optical beam path and neutral density filters were used resulting in reduction of the maximum available laser power to 7 mW. Samples at the microscope stage were positioned remotely with a joystick using an encoded, motorized *XYZ* translation stage (0.1 µm step size) controlled by a Prior Scientific ProScan II controller. WiRE 3.2 software, operating on a bench top computer, was used for instrument control and data collection. Before all measurements, the instrument was wavelength calibrated using an internal silicon standard. Data analysis was completed using IgorPro 6.0 software (Wavemetrics).[102]

3. RESULTS AND DISCUSSION

The Army and first responders have a keen interest in identifying potential hazards on a host of commonly encountered items/substrates. With this in mind, we were interested to determine if when using the inkjet system, it would be possible to fabricate AN materials on various surfaces and detect the printed materials. To test this hypothesis the experiments discussed in the following sections were conducted.

Table 1. Example print setting (standard wave) for an AN mass droplet of 9.90 x 10^{-3} µg sample.

Print Parameters	
System Parameter	System Setting
Dwell	34
Echo	32
Dwell Voltage	21
Echo Voltage	-19
Set point	-0.07

To characterize how AN samples set up on various materials, we inkjet printed several concentrations of AN onto silicon, aluminum, polyethylene, various cloth materials, and human hair substrates. These materials all have different wicking capabilities and rigidness, and are therefore assumed to interact differently with the printed AN solution. The printed materials were physically characterized with SEM measurements, and were also spectrally characterized by Raman measurements. The results for these various experiments will be discussed in the following sections.

Table 2. Print settings for an AN mass droplet of 9.90e-3 µg sample.

Sample	AN Concentration	# drops	Spacing	X,Y Drops
A	10 µg/cm^2	1.04E+05	0.314	241, 161
B	1000 µg/cm^2	1.04E+06	0.0995	765, 161

In these experiments a high and low concentration of AN was inkjet printed onto the following surfaces: silicon, aluminum, polyethylene, cloth materials, velveteen, tarp, and human hair. These materials were selected as they represent both natural and manmade materials. The parameters used for inkjet printing the sample are listed in Table 1. For these inkjetted materials, a standard wave form was used with a dwell time set at 34 µs, echo time at 32 µs, dwell voltage at 21 V, echo voltage at -19 V, and a pressure set point set at -0.07 psi. Using these settings, it was possible to consistently produce a uniform droplet. To print the materials at the two desired concentrations, the parameters in Table 2 were followed. For these experiments both the spacing and number of drops in the X direction were varied to produce a final sample concentration of 10 µg/cm^2 (representing trace) and 1000 µg/cm^2 (representing bulk). For these experiments, and AN solution concentration of 1.20 M was simultaneously inkjet printed onto the substrate surfaces under investigation.

Downloaded From: http://proceedings.spiedigitallibrary.org/ on 08/24/2015 Terms of Use: http://spiedigitallibrary.org/ss/TermsOfUse.aspx

To characterize how the printed material "looked" on the substrate surface a series of digital camera and SEM images were collected. See Figure 3 for an example photographand SEM image of substrate materials onto which AN was printed. In Figure 3, photo and SEM images of (A, B) velveteen, (C, D) cloth, (E, F) hair, (G, H) Tarp, (I,J) aluminum, (K, L) silicon, and (M,N) PE are shown. These materials have AN printed on them at concentrations of either 10 ug/cm^2 or 1000 ug/cm^2. In SEM figure B, D, F, and H it is challenging to see the printed AN material on the substrate surface. This may be due to some of these materials being more "absorbent" of wet materials (B, D, F) as compared to some of the more rigid surfaces (J, L, N). Also, due to the surface interactions between the substrate and the AN, physically different depositions of AN appear to have formed on some of the more rigid surfaces. For comparison, consider J, L and N (all printed under same conditions at same time). In these SEM images, the AN printed materials appear as either "crunchy" rows, a random dispersion of large and small features, or a somewhat uniform (size and spacing) array of material.

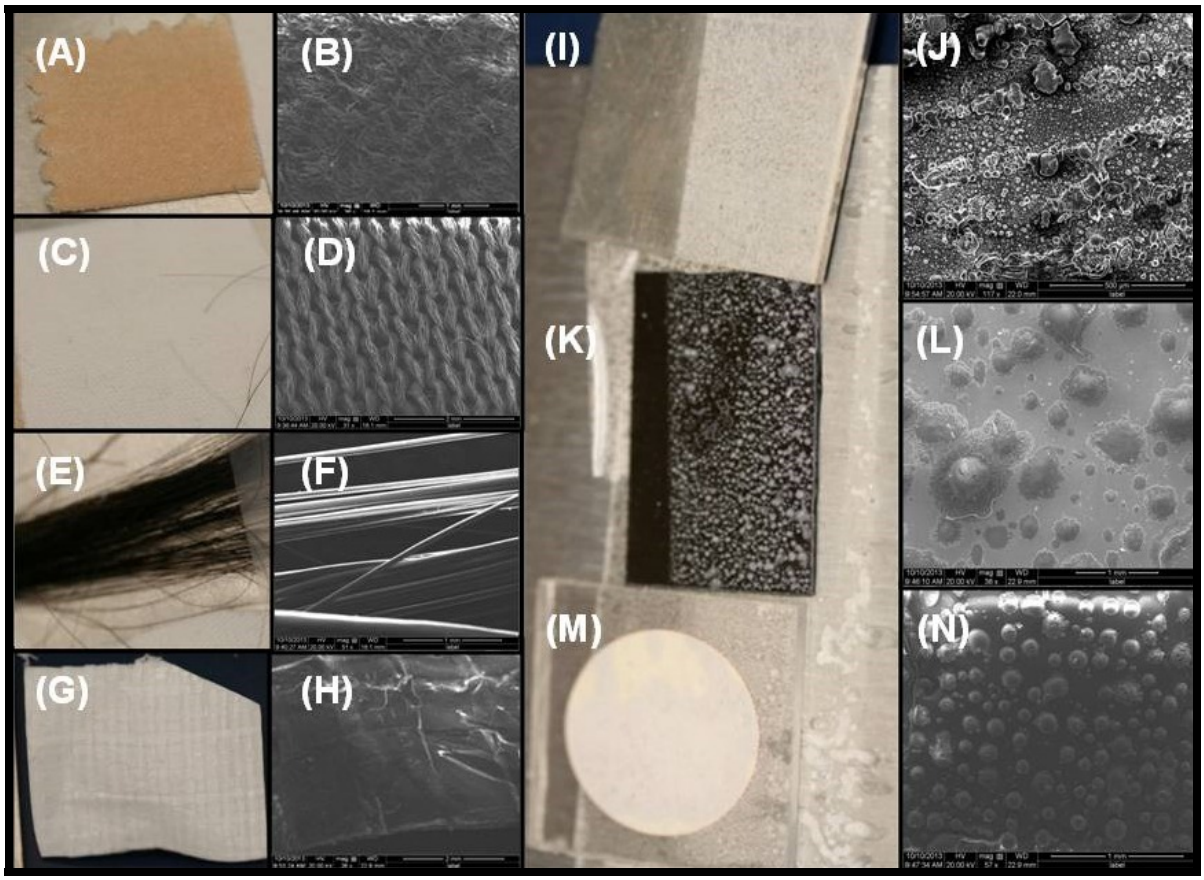

Figure. 3. Photo and SEM images of (A, B) velveteen, (C, D) cloth, (E, F) hair, (G, H) Tarp, (I,J) aluminum, (K, L) silicon, and (M, N) PE. These materials have AN printed on them at concentrations of either 10 ug/cm^2 or 1000 ug/cm^2. Due to the surface interactions between the substrate and the AN, physically different depositions of AN appear to have formed, compare J, K and M (all printed under same conditions at same time).

To physically characterize the nature of the actual AN droplet on a rigid surface, SEM images were collected of individual AN deposits. In Figure 4A, a representative AN droplet from a 10 µg/cm^2 printed surface concentration is shown. This droplet is approximately 50 µm in diameter, and appears to have an outer surface that is crystalline in structure. This image is an example of how the uniform droplets generally appear when printed on a rigid surface with adequate spacing and drying times.

For all Raman measurements, it was necessary to first determine a spectral baseline of the substrate material, and then collect data from the two deposited AN concentrations. In Figure 4B-D, the Raman data for a baseline substrate (Si, Al and PE), and printed 10 µg/cm^2 AN, and 1000 µg/cm^2 AN concentration are all shown. In Figure 4B, Raman silicon has

Downloaded From: http://proceedings.spiedigitallibrary.org/ on 08/24/2015 Terms of Use: http://spiedigitallibrary.org/ss/TermsOfUse.aspx

a broad band located between 922 cm^{-1} and 1000 cm^{-1}. The signal of the 1000 $\mu g/cm^2$ AN as compared to the 10 $\mu g/cm^2$ AN is approximately 9X larger. The starred peak reflects the AN band symmetric stretch mode of NO_3^- located at 1043.2 cm^{-1} for the 10 $\mu g/cm^2$ Raman band, and 1044.2 cm^{-1} for the 1000 $\mu g/cm^2$ Raman band. In Figure 4C, the background and Raman data for AN on aluminum is shown. In this figure, the starred band is located at 1042.3 cm^{-1} for the 10 $\mu g/cm^2$ Raman band, and 1044.2 cm^{-1} for the 1000 $\mu g/cm^2$ Raman band. Polyethylene (Figure 4D) has main bands occurring at 630.47 cm^{-1}, 702.99 cm^{-1}, 857.08 cm^{-1}, 1117.1 cm^{-1}, 1175.0 cm^{-1}, 1283.60 (C-H twisting) cm^{-1}, 1614.1 cm^{-1}, and 1724.60 cm^{-1}. In this figure, the starred band is located at 1042.3 cm^{-1} for AN.

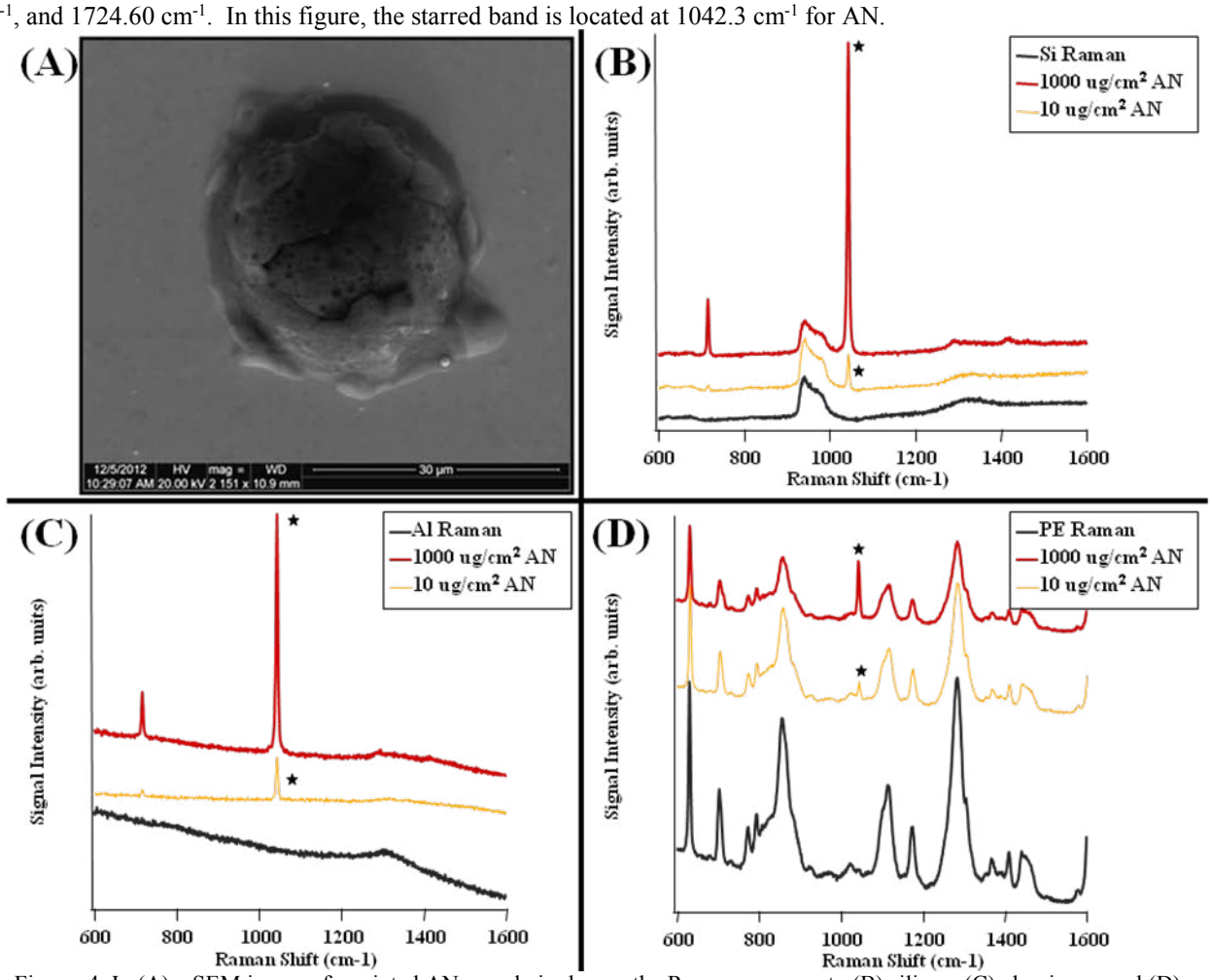

Figure. 4. In (A) a SEM image of a printed AN sample is shown, the Raman response to (B) silicon, (C) aluminum, and (D) polyethylene plastic is shown. In (B to D), the spectral Raman signatures from the blank material, 1000 $\mu g/cm^2$, and 10 $\mu g/cm^2$ AN printed samples are shown. The main AN band is designated with a star.

In Figure 5A-D, the Raman data for a baseline, 10 $\mu g/cm^2$ AN, and 1000 $\mu g/cm^2$ AN concentration are all shown for cloth, velveteen, plastic tarp material, and finally human hair. In Figure 5A, the spectral data for cloth is shown. Cloth has main Raman bands located at 631.49 cm^{-1}, 702.99 cm^{-1}, 859.05 cm^{-1}, 999.24 cm^{-1}, 1095.4 cm^{-1}, 1291.8 cm^{-1}, 1418.4 cm^{-1}, 1615.8 cm^{-1}, and 1727.9 cm^{-1}. In this figure, the starred band is located at 1043.3 cm^{-1} for the 1000 $\mu g/cm^2$ AN sample. The lower concentration AN was not detectable for this material. In figure 5B, the spectral data for velveteen is shown. Velveteen has background Raman bands located at 1096.4 $cm^{-1}$and 1121.8 cm^{-1}. Velveteen with 1000 $\mu g/cm^2$ AN has a main band located at 1043.3 cm^{-1}. No AN was detectable at the lower concentration on cloth or velveteen. It is possible that because of the absorbent nature of these materials, the AN solution is being wicked into the material. Therefore the lower concentration AN deposits are much more challenging to detect as compared to the higher bulk concentration.

Downloaded From: http://proceedings.spiedigitallibrary.org/ on 08/24/2015 Terms of Use: http://spiedigitallibrary.org/ss/TermsOfUse.aspx

In Figure 5C, Raman data for plastic tarp material is shown. Tarp has spectral bands located at 608.83 cm^{-1}, 1062.3 cm^{-1}, 1086.0 cm^{-1}, 1128.4 cm^{-1}, 1295.4 cm^{-1}, 1416.6 cm^{-1}, and 1439.6 cm^{-1}. In this figure, the starred band is located at 1042.3 cm^{-1} for the 10 $\mu g/cm^2$ AN sample, and 1044.2 cm^{-1} for the 1000 $\mu g/cm^2$ AN sample. This slight shift in band location may be attributable to some moisture in the sample still being present, but is being characterized as predominately phase IV material. In Figure 4D, the Raman spectral data from human hair is shown. In this figure, there is significant fluorescence background from the material. Due to the large background fluorescence, only the higher concentration 1000 $\mu g/cm^2$ AN sample has a measurable Raman band located at 1044.20 cm^{-1} (under the test conditions outlined in this proceedings paper).

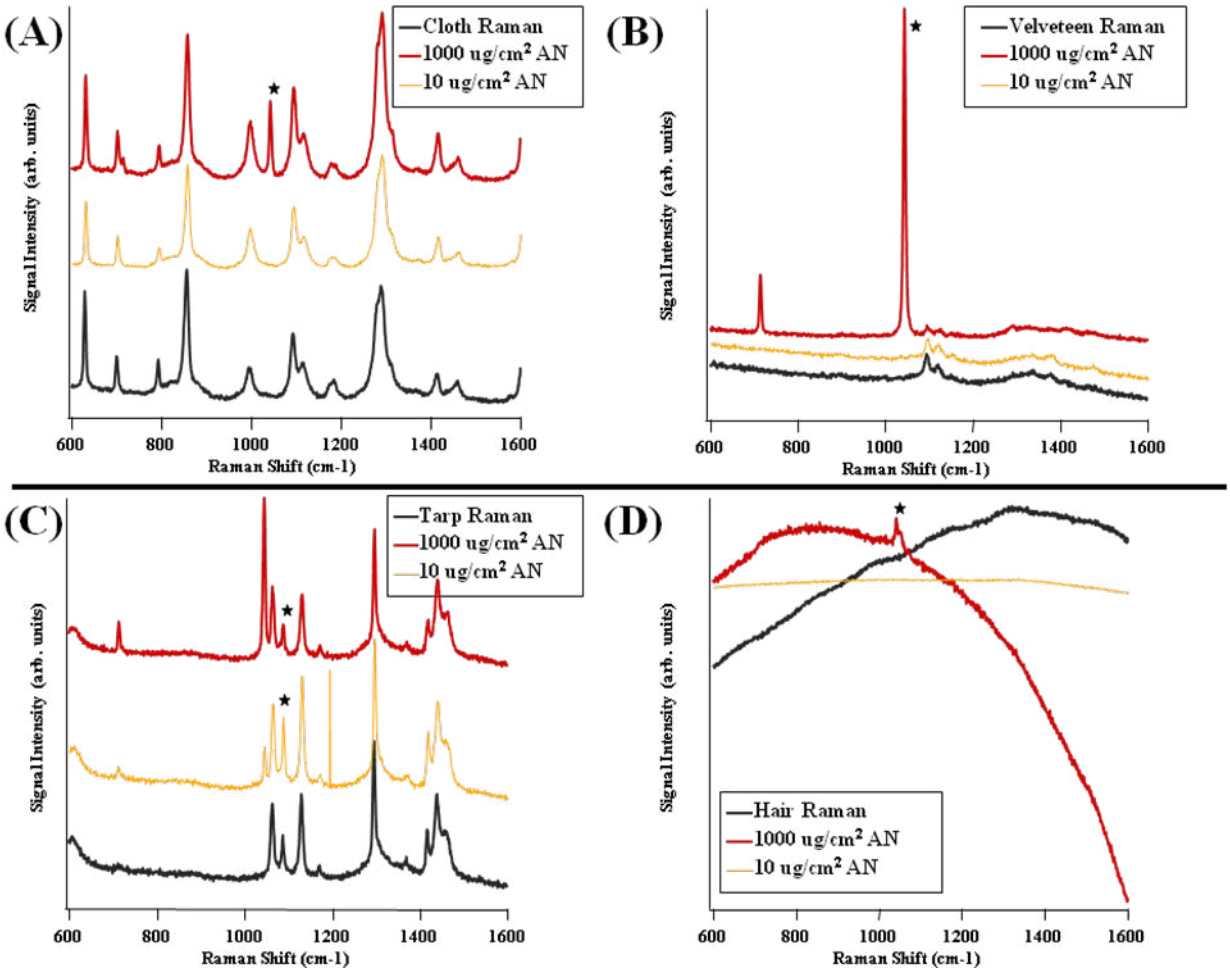

Figure 5. The Raman response to (A) cloth, (B) Veleveteen, (C) tarp, and (D) human hair is shown. The spectral Raman signatures from the blank material, 1000 $\mu g/cm^2$, and 10 $\mu g/cm^2$ AN printed samples are shown. The main AN band is designated with a star.

Table 2. Summary Raman signatures collected from several substrates inkjetted with AN at different concentrations.

Downloaded From: http://proceedings.spiedigitallibrary.org/ on 08/24/2015 Terms of Use: http://spiedigitallibrary.org/ss/TermsOfUse.aspx

Substrate Type	Background Material Raman Bands	AN Raman 10 µg/cm^2	AN Raman 100 µg/cm^2
Silicon	Broad band located between 922 cm^{-1} and 1000 cm^{-1}	1043.2 cm^{-1} Phase IV AN	1044.2 cm^{-1} Phase IV AN
Aluminum	1303.6 cm^{-1}	1042.3 cm^{-1} Phase IV AN	1044.2 cm^{-1} Phase IV AN
Polyethylene	630.47 cm^{-1}, 702.99 cm^{-1}, 857.08 cm^{-1}, 1117.1 cm^{-1}, 1175.0 cm^{-1}, 1283.60 (C-H twisting) cm^{-1}, 1614.1 cm^{-1}, and 1724.60 cm^{-1}	1042.3 cm^{-1} Phase IV AN	1042.3 cm^{-1} Phase IV AN
Cloth	631.49 cm^{-1}, 702.99 cm^{-1}, 859.05 cm^{-1}, 999.24 cm^{-1}, 1095.4 cm^{-1}, 1291.8 cm^{-1}, 1418.4 cm^{-1}, 1615.8 cm^{-1}, and 1727.9 cm^{-1}.	Not detectable	1043.3 cm^{-1} Phase IV AN
Velveteen	1096.4 cm^{-1}and 1121.8 cm^{-1}	Not detectable	1043.3 cm^{-1} Phase IV AN
Tarp	608.83 cm^{-1}, 1062.3 cm^{-1}, 1086.0 cm^{-1}, 1128.4 cm^{-1}, 1295.4 cm^{-1}, 1416.6 cm^{-1}, and 1439.6 cm^{-1}	1042.3 cm^{-1} Phase IV AN	1044.2 cm^{-1} Phase IV AN
Human Hair	Broad Fluorescence band	Not detectable	1044.20 cm^{-1} Phase IV AN

4. CONCLUSIONS AND FUTURE WORKS

In this proceedings paper, efforts to characterize the nature of AN signatures observed on several different types of substrate were conducted. AN was inkjet printed onto several common materials (silicon, aluminum, polyethylene, various cloth materials, and human hair) at both bulk (>100 µg/cm^2) and trace (<100 µg/cm^2) concentrations. We were able to demonstrate that trace AN could be measured on several of the surfaces, and characterize the AN phase present (generally phase IV was observed). Please remember that from these measurements, no attempt was made to characterize the starting analyte material, or comment on how the sample handling methods may impact the final product measured.

As described in the results section, we were able to measure trace AN inkjet deposited onto the following materials silicon, aluminum, polyethylene, and various cloth materials. Bulk AN material was able to be measured on the following substrate surfaces: silicon, aluminum, polyethylene, various cloth materials, and human hair.

Accurately training standoff detection systems for energetic hazards materials remains a priority. While AN is still extensively used, due to the increased restrictions on the import of it into theatre, a new threat is emerging, potassium chlorate. According to the a more recent article in USA today,[103] "*Potassium chlorate has surpassed fertilizer as the explosive of choice for insurgents, Pentagon research shows. For the first time in the 12-year war, potassium chlorate was the most common ingredient, fueling 60% of the IEDs.*" Just as with AN, it is necessary to understand how working with this material and inkjet depositing it onto surfaces may impact the specific Raman signatures that are measured. Future works will include characterizing other common IED precursors to better understand how they interact with their environment.

Downloaded From: http://proceedings.spiedigitallibrary.org/ on 08/24/2015 Terms of Use: http://spiedigitallibrary.org/ss/TermsOfUse.aspx

REFERENCES

[1] H. Brust, S. Willemse, T. Zeng, A. van Asten, M. Koeberg, A. van der Heijden *et al.*, "Impurity profiling of trinitrotoluene using vacuum-outlet gas chromatography-mass spectrometry," Journal of Chromatography A 1374, 224 (2014).

[2] R. Laudien, D. Riebe, T. Beitz, H. G. Lohmannsroben, "Detection of explosive related nitroaromatic compounds (ERNC) by laser-based ion mobility spectrometry," Proceedings of the SPIE - The International Society for Optical Engineering 7116, 71160T (9 pp.) (2008).

[3] M. Tabrizchi, V. Ilbeigi, "Detection of explosives by positive corona discharge ion mobility spectrometry," Journal of Hazardous Materials 176, 692 (2010).

[4] J. Tomlinson-Phillips, A. Wooten, J. Kozole, J. Deline, P. Beresford, J. Stairs, "Characterization of TATP gas phase product ion chemistry via isotope labeling experiments using ion mobility spectrometry interfaced with a triple quadrupole mass spectrometer," Talanta 127, 152 (2014).

[5] A. Dicken, A. Shevchuk, K. Rogers, S. Godber, P. Evans, "High energy transmission annular beam X-ray diffraction," Optics Express 23, 6304 (2015).

[6] S. Kolkoori, N. Wrobel, S. Hohendorf, B. Redmer, U. Ewert, "Mobile High-energy X-ray Radiography for Nondestructive Testing of Cargo Containers," Materials Evaluation 73, 175 (2015).

[7] K. Bergaoui, N. Reguigui, C. K. Gary, C. Brown, J. T. Cremer, J. H. Vainionpaa *et al.*, "Monte Carlo simulation of explosive detection system based on a Deuterium-Deuterium (D-D) neutron generator," Applied Radiation and Isotopes 94, 118 (2014).

[8] H.-J. Im, Y.-H. Lee, B. C. Song, Y. J. Park, "One-Step Detection of Explosives Using a Self-Developed Computer Program Based on Application of a Principal Component Analysis in Prompt gamma-Spectra," Asian Journal of Chemistry 26, 4081 (2014).

[9] J. E. McFee, A. A. Faust, H. R. Andrews, E. T. H. Clifford, C. M. Mosquera, "Performance of an improved thermal neutron activation detector for buried bulk explosives," Nuclear Instruments & Methods in Physics Research Section a-Accelerators Spectrometers Detectors and Associated Equipment 712, 93 (2013).

[10] D. Sudac, S. Majetic, K. Nad, J. Obhodas, V. Valkovic, "Improved System for Inspecting Minefields and Residual Explosives," Ieee Transactions on Nuclear Science 61, 2195 (2014).

[11] Z. D. Whetstone, K. J. Kearfott, "A review of conventional explosives detection using active neutron interrogation," Journal of Radioanalytical and Nuclear Chemistry 301, 629 (2014).

[12] I. A. Buryakov, T. I. Buryakov, V. T. Matsaev, "Optical chemical sensors for the detection of explosives and associated substances," Journal of Analytical Chemistry 69, 616 (2014).

[13] S. Parajuli, W. Miao, "Sensitive Determination of Triacetone Triperoxide Explosives Using Electrogenerated Chemiluminescence," Analytical Chemistry 85, 8008 (2013).

[14] J. Y. Park, L. J. Kricka, "Prospects for the commercialization of chemiluminescence-based point-of-care and on-site testing devices," Analytical and Bioanalytical Chemistry 406, 5631 (2014).

[15] F. S. Romolo, E. Ferri, M. Mirasoli, M. D'Elia, L. Ripani, G. Peluso *et al.*, "Field detection capability of immunochemical assays during criminal investigations involving the use of TNT," Forensic Science International 246, 25 (2015).

[16] L. Xiaohua, Z. Zhujun, T. Liang, "A novel array of chemiluminescence sensors for sensitive, rapid and high-throughput detection of explosive triacetone triperoxide at the scene," Biosensors and Bioelectronics 47, 356 (2013).

[17] G. V. Zyryanov, D. S. Kopchuk, I. S. Kovalev, E. V. Nosova, V. L. Rusinov, O. N. Chupakhin, "Chemosensors for detection of nitroaromatic compounds (explosives)," Russian Chemical Reviews 83, 783 (2014).

[18] D. Garcia-Romeo, I. Pellejero, M. A. Urbiztondo, J. Sese, M. P. Pina, P. A. Martinez *et al.*, "Portable low-power electronic interface for explosive detection using microcantilevers," Sensors and Actuators B-Chemical 200, 31 (2014).

[19] D. Lee, S. Kim, S. Jeon, T. Thundat, "Direct Detection and Speciation of Trace Explosives Using a Nanoporous Multifunctional Microcantilever," Analytical Chemistry 86, 5077 (2014).

[20] P. Ray, S. Pandey, V. R. Rao, "Development of graphene nanoplatelet embedded polymer microcantilever for vapour phase explosive detection applications," Journal of Applied Physics 116, (2014).

[21] D. Strle, B. Stefane, E. Zupanic, M. Trifkovic, M. Macek, G. Jaksa *et al.*, "Sensitivity Comparison of Vapor Trace Detection of Explosives Based on Chemo-Mechanical Sensing with Optical Detection and Capacitive Sensing with Electronic Detection," Sensors 14, 11467 (2014).

Downloaded From: http://proceedings.spiedigitallibrary.org/ on 08/24/2015 Terms of Use: http://spiedigitallibrary.org/ss/TermsOfUse.aspx

[22] A. Concha, D. S. Mills, A. Feugier, H. Zulch, C. Guest, R. Harris *et al.*, "Using Sniffing Behavior to Differentiate True Negative from False Negative Responses in Trained Scent-Detection Dogs," Chemical Senses 39, 749 (2014).
[23] W. Kranz, K. Kitts, N. Strange, J. Cummins, E. Lotspeich, J. Goodpaster, "On the smell of Composition C-4," Forensic Science International 236, 157 (2014).
[24] Y. Oh, Y. Lee, J. Heath, M. Kim, "Applications of Animal Biosensors: A Review," Ieee Sensors Journal 15, 637 (2015).
[25] T. Onodera, K. Toko, "Towards an Electronic Dog Nose: Surface Plasmon Resonance Immunosensor for Security and Safety," Sensors 14, 16586 (2014).
[26] J. Wang, L. Yang, B. Liu, H. Jiang, R. Liu, J. Yang *et al.*, "Inkjet-Printed Silver Nanoparticle Paper Detects Airborne Species from Crystalline Explosives and Their Ultratrace Residues in Open Environment," Analytical Chemistry 86, 3338 (2014).
[27] M. K. Habib, "Controlled biological and biomimetic systems for landmine detection," Biosensors & Bioelectronics 23, 1 (2007).
[28] J. A. Shaw, N. L. Seldomridge, D. L. Dunkle, P. W. Nugent, L. H. Spangler, J. J. Bromenshenk *et al.*, "Lidar measurements of honey bees for locating land mines," Optics & Photonics News 16, 33 (2005).
[29] B. Wen, H. Eilers, "Potential interference mechanism for the detection of explosives via laser-based standoff techniques," Appl. Phys. B-Lasers O. 106, 473 (2012).
[30] M. Mashal, in *World Time* Time, Ed. (Kandahar, 2013), vol. 2013.
[31] B. D. Piorek, S. J. Lee, M. Moskovits, C. D. Meinhart, "Free-Surface Microfluidics/Surface-Enhanced Raman Spectroscopy for Real-Time Trace Vapor Detection of Explosives," Anal. Chem. 84, 9700 (2012).
[32] E. L. Holthoff, M. E. Farrell, P. M. Pellegrino "Investigating a drop-on-demand microdispenser for standardized sample preparation," SPIE 8358:, 83580V (2012).
[33] C. De Perre, A. Prado, B. R. McCord, "Rapid and specific detection of urea nitrate and ammonium nitrate by electrospray ionization time-of-flight mass spectrometry using infusion with crown ethers," Rapid Commun. Mass Sp. 26, 154 (2012).
[34] A. Chou, E. Jaatinen, R. Buividas, G. Seniutinas, S. Juodkazis, E. L. Izake *et al.*, "SERS substrate for detection of explosives," Nanoscale 4, 7419 (2012).
[35] A. Banas, K. Banas, M. B. H. Breese, J. Loke, B. H. Teo, S. K. Lim, "Detection of microscopic particles present as contaminants in latent fingerprints by means of synchrotron radiation-based Fourier transform infra-red micro-imaging," Analyst 137, 3459 (2012).
[36] B. Zachhuber, G. Ramer, A. Hobro, E. T. H. Chrysostom, B. Lendl, "Stand-off Raman spectroscopy: a powerful technique for qualitative and quantitative analysis of inorganic and organic compounds including explosives," Anal. Bioanal. Chem. 400, 2439 (2011).
[37] A. Tripathi, E. D. Emmons, P. G. Wilcox, J. A. Guicheteau, D. K. Emge, S. D. Christesen *et al.*, "Semi-Automated Detection of Trace Explosives in Fingerprints on Strongly Interfering Surfaces with Raman Chemical Imaging," Appl. Spectros. 65, 611 (2011).
[38] H. Ostmark, M. Nordberg, T. E. Carlsson, "Stand-off detection of explosives particles by multispectral imaging Raman spectroscopy," Appl. Optics 50, 5592 (2011).
[39] D. D. Tuschel, A. V. Mikhonin, B. E. Lemoff, S. A. Asher, "Deep Ultraviolet Resonance Raman Excitation Enables Explosives Detection," Appl. Spectrosc. 64, 425 (2010).
[40] F. T. Docherty, P. B. Monaghan, C. J. McHugh, D. Graham, W. E. Smith, J. M. Cooper, "Simultaneous multianalyte identification of molecular species involved in terrorism using Raman spectroscopy," IEEE Sens. J. 5, 632 (2005).
[41] I. R. Lewis, N. W. Daniel, P. R. Griffiths, "Interpretation of Raman spectra of nitro-containing explosive materials. Part I: Group frequency and structural class membership," Applied Spectroscopy 51, 1854 (1997).
[42] T. F. Chen, S. H. Lu, A. J. Wang, D. Zheng, Z. L. Wu, Y. S. Wang, "Detection of explosives by surface enhanced Raman scattering using substrate with a monolayer of ordered Au nanoparticles," Applied Surface Science 317, 940 (2014).
[43] Z. Gong, H. Du, F. Cheng, C. Wang, C. Wang, M. Fan, "Fabrication of SERS Swab for Direct Detection of Trace Explosives in Fingerprints," Acs Applied Materials & Interfaces 6, 21931 (2014).
[44] A. K. M. Jamil, E. L. Izake, A. Sivanesan, P. M. Fredericks, "Rapid detection of TNT in aqueous media by selective label free surface enhanced Raman spectroscopy," Talanta 134, 732 (2015).

Downloaded From: http://proceedings.spiedigitallibrary.org/ on 08/24/2015 Terms of Use: http://spiedigitallibrary.org/ss/TermsOfUse.aspx

[45] J. C. Carter, S. M. Angel, M. Lawrence-Snyder, J. Scaffidi, R. E. Whipple, J. G. Reynolds, "Standoff detection of high explosive materials at 50 meters in ambient light conditions using a small Raman instrument," Applied Spectroscopy 59, 769 (2005).

[46] D. S. Moore, "Instrumentation for trace detection of high explosives," Review of Scientific Instruments 75, 2499 (2004).

[47] J. I. Steinfeld, J. Wormhoudt, "Explosives detection: A challenge for physical chemistry," Annual Review of Physical Chemistry 49, 203 (1998).

[48] J. Guicheteau, S. Christesen, A. Tripathi, E. Emmons, D. Emge, P. Wilcox *et al.*, "Raman and Surface-enhanced Raman for Military Applications," AIP Conf. Proc. 1267, 1069 (2010).

[49] J. Moros, J. A. Lorenzo, J. J. Laserna, "Standoff detection of explosives: critical comparison for ensuing options on Raman spectroscopy-LIBS sensor fusion," Anal. Bioanal. Chem. 400, 3353 (2011).

[50] S. Wallin, A. Pettersson, H. Ostmark, A. Hobro, "Laser-based standoff detection of explosives: a critical review," Anal. Bioanal. Chem. 395, 259 (2009).

[51] J. Moros, J. Antonio Lorenzo, P. Lucena, L. Miguel Tobaria, J. Javier Laserna, "Simultaneous Raman Spectroscopy-Laser-induced Breakdown Spectroscopy for Instant Standoff Analysis of Explosives Using a Mobile Integrated Sensor Platform," Anal. Chem. 82, 1389 (2010).

[52] X.-M. Lin, Y. Cui, Y.-H. Xu, B. Ren, Z.-Q. Tian, "Surface-enhanced Raman spectroscopy: substrate-related issues," Analytical and Bioanalytical Chemistry 394, 1729 (2009).

[53] J. Oxley, J. Smith, J. Brady, F. Dubnikova, R. Kosloff, L. Zeiri *et al.*, "Raman and infrared fingerprint spectroscopy of peroxide-based explosives," Appl. Spectrosc. 62, 906 (2008).

[54] E. D. Emmons, A. Tripathi, J. A. Guicheteau, S. D. Christesen, A. W. Fountain, III, "Raman Chemical Imaging of Explosive-Contaminated Fingerprints," Appl. Spectrosc. 63, 1197 (2009).

[55] C. Song, J. D. Driskell, R. A. Tripp, Y. Cui, Y. Zhao, in *Chemical, Biological, Radiological, Nuclear, and Explosives,* A. W. Fountain, Ed. (2012), vol. 8358.

[56] E. L. Holthoff, D. N. Stratis-Cullum, M. E. Hankus, "Xerogel-Based Molecularly Imprinted Polymers for Explosives Detection," SPIE 7665, (2010).

[57] J. I. J. Rozo, M. d. R. Balaguara, A. Cabanzo, E. d. l. C. Montoya, S. P. Hernadez-Rivera, "Enhanced Raman scattering of nitro-explosives on nanoparticle substrates: Au-Ag alloy, tin oxide, and scandium oxide," SPIE 6201, 62012G1 (2006).

[58] E. D. Emmons, J. A. Guicheteau, A. W. Fountain, III, S. D. Christesen, "Comparison of Visible and Near-Infrared Raman Cross-Sections of Explosives in Solution and in the Solid State," Appl Spectros 66, 636 (2012).

[59] M. E. Farrell, E. L. Holthoff, P. M. Pellegrino, "Next generation Surface Enhanced Raman Scattering (SERS) substrates for Hazard Detection," SPIE 8358, 835816 (2012).

[60] C. K. Chan, M. N. Chan, "New Directions: Polymorphic transformation of ammonium nitrate in atmospheric aerosols," Atmos. Eviron. 38, 1387 (2004).

[61] C. S. Choi, J. E. Mapes, E. Prince, "Structure of ammonium nitrate (IV)," Acta Crystal. Sect. B-Struct. Cryst. Cryst.Chem. 28, 1357 (1972).

[62] R. J. Davey, P. D. Guy, A. J. Ruddick, "The IV- III polymophic phase transition in aqueous slurries of ammonium nitrate " J. Col. Interf. Sci. 108, 189 (1985).

[63] R. J. Davey, A. J. Ruddick, P. D. Guy, B. Mitchell, S. J. Maginn, L. A. Polywka, "The IV-III polymorphic phase-transition in ammonium nitrate - a unique example of solvent mediation," J. Phys. D. Apply. Phys 24, 176 (1991).

[64] M. E. Farrell, E. L. Holthoff, P. M. Pellegrino, "Surface-Enhanced Raman Scattering Detection of Ammonium Nitrate Samples Fabricated Using Drop-on-Demand Inkjet Technology," Appl. Spec. 68, 287 (2014).

[65] R. M. Harrison, W. T. Sturgis, A.-M. N. Kitto, Y. Li, "Kinetics of Evaporation of Ammonium chloride and ammonium Nitrate Aerosols," Atmos. Environ. 24, 1883 (1990).

[66] J. R. Holden, C. W. Dickinson, "Crystal Structure of 2 solid solution phases of ammonium nitrate and pottasium nitrate," J. Phys. Chem. 79, 249 (1975).

[67] C. B. Richardson, R. L. Hightower, "Evaporation of ammonium nitrate particles," Atmos. Envir. 21, 971 (1987).

[68] E. D. Emmons, M. E. Farrell, E. L. Holthoff, A. Tripanthi, N. Green, R. P. Moon *et al.*, "Characterization of Polymorphic States in Energetic Samples of 1,3,5-Trinitro-1,3,5-Triazine (RDX) Fabricated Using Drop-on-Demand Inkjet Technology," Appl. Spectrosc. 66, 628 (2012).

Downloaded From: http://proceedings.spiedigitallibrary.org/ on 08/24/2015 Terms of Use: http://spiedigitallibrary.org/ss/TermsOfUse.aspx

[69] E. D. Emmons, M. E. Farrell, E. L. Holthoff, A. Tripathi, N. Green, R. P. Moon *et al.*, "Characterization of Polymorphic States in Energetic Samples of 1,3,5-Trinitro-1,3,5-Triazine (RDX) Fabricated Using Drop-on-Demand Inkjet Technology," Applied Spectroscopy 66, 628 (2012).

[70] M. Ghosh, L. Wang, S. A. Asher, "Deep-Ultraviolet Resonance Raman Excitation Profiles of NH4NO3, PETN, TNT, HMX, and RDX," Applied Spectroscopy 66, 1013 (2012).

[71] P. Torres, L. Mercado, I. Cotte, S. P. Hernadez, N. Mina, A. Santana *et al.*, "Vibrational Spectroscopy Study of B and A RDX Deposits," J. Phys. Chem. B 108, 8799 (2004).

[72] P. Torres, L. Mercado, L. Mortimer, N. Mina, S. Hernandez, R. Larau *et al.*, "Raman and scanning electron microscopy measurements of RDX on glass substrates," SPIE 5089, 1054 (2003).

[73] D. Bedrov, C. Ayyagari, G. D. Smith, T. D. Sewell, R. Menikoff, J. M. Zaug, "Molecular dynamics simulations of HMX crystal polymorphs using a flexible molecule force field," Journal of Computer-Aided Materials Design 8, 77 (2001).

[74] W. Zhu, J. Xiao, G. Ji, F. Zhao, H. Xiao, "First-principles study of the four polymorphs of crystalline octahydro-1,3,5,7-tetranitro-1,3,5,7-tetrazocine," Journal of Physical Chemistry B 111, 12715 (2007).

[75] M. Abdelhamid, F. J. Fortes, M. A. Harith, J. J. Laserna, "Analysis of explosive residues in human fingerprints using optical catapulting-laser-induced breakdown spectroscopy," Journal of Analytical Atomic Spectrometry 26, 1445 (2011).

[76] E. D. Emmons, A. Tripathi, J. A. Guicheteau, S. D. Christesen, A. W. Fountain, III, "Raman Chemical Imaging of Explosive-Contaminated Fingerprints," Applied Spectroscopy 63, 1197 (2009).

[77] P. Jander, R. Noll, "Automated Detection of Fingerprint Traces of High Explosives Using Ultraviolet Raman Spectroscopy," Applied Spectroscopy 63, 559 (2009).

[78] P. Lucena, I. Gaona, J. Moros, J. J. Laserna, "Location and detection of explosive-contaminated human fingerprints on distant targets using standoff laser-induced breakdown spectroscopy," Spectrochimica Acta Part B-Atomic Spectroscopy 85, 71 (2013).

[79] Y. Mou, J. W. Rabalais, "Detection and Identification of Explosive Particles in Fingerprints Using Attenuated Total Reflection-Fourier Transform Infrared Spectromicroscopy," Journal of Forensic Sciences 54, 846 (2009).

[80] J. Oxley, J. Smith, J. Brady, F. Dubnikova, R. Kosloff, L. Zeiri *et al.*, "Raman and infrared fingerprint spectroscopy of peroxide-based explosives," Applied Spectroscopy 62, 906 (2008).

[81] D. J. Phares, J. K. Holt, G. T. Smedley, R. C. Flagan, "Method for characterization of adhesion properties of trace explosives in fingerprints and fingerprint simulations," Journal of Forensic Sciences 45, 774 (2000).

[82] A. Tripathi, E. D. Emmons, P. G. Wilcox, J. A. Guicheteau, D. K. Emge, S. D. Christesen *et al.*, "Semi-Automated Detection of Trace Explosives in Fingerprints on Strongly Interfering Surfaces with Raman Chemical Imaging," Applied Spectroscopy 65, 611 (2011).

[83] J. R. Verkouteren, J. L. Coleman, I. Cho, "Automated Mapping of Explosives Particles in Composition C-4 Fingerprints," Journal of Forensic Sciences 55, 334 (2010).

[84] J. R. Verkouteren, J. Lawrence, G. A. Klouda, M. Najarro, J. Grandner, R. M. Verkouteren *et al.*, "Performance metrics based on signal intensity for ion mobility spectrometry - based explosive trace detectors using inkjet printed materials," Analyst 139, 5488 (2014).

[85] E. Windsor, M. Najarro, A. Bloom, B. Benner, Jr., R. Fletcher, R. Lareau *et al.*, "Application of Inkjet Printing Technology to Produce Test Materials of 1,3,5-Trinitro-1,3,5 Triazcyclohexane for Trace Explosive Analysis," Analytical Chemistry 82, 8519 (2010).

[86] M. E. Farrell, E. L. Holthoff, P. M. Pellegrino, "Surface-Enhanced Raman Scattering Detection of Ammonium Nitrate Samples Fabricated Using Drop-on-Demand Inkjet Technology," Applied Spectroscopy 68, 287 (2014).

[87] S. Kettle, "The Raman spectra of Phase III ammonium nitrate" (Air Force Office of Scientific Research (AFSC) USAF, 1982).

[88] A. Savara, M. J. Li, W. M. H. Sachtler, E. Weitz, "Catalytic reduction of NH4NO3 by NO: Effects of solid acids and implications for low temperature DeNO(x) processes," Appl. Catal. B-Environ. 81, 251 (2008).

[89] J. M. J. A. d. Brugh, J. S. Henzing, M. Schaap, W. T. Morgan, C. C. v. Heerwaarden, E. P. Weijers *et al.*, "Modelling the partitioning of ammonium nitrate in the convective boundary layer," Atmos. Chem. Phys., 12, 3005 (2012).

[90] A. W. Stelson, J. H. Seinfeld, "Relative humidity and temperature dependence of the ammonium nitrate dissociation constant," Atmos. Environ. 16, 983 (1982).

[91] R. M. Harrison, W. T. Sturges, Y. L. A.-M.N. Kitto, "Kinetics of evaporation of ammonium chloride and ammonium nitrate aerosols," Atmos. Envir., 24A, 1883 (1990).

Downloaded From: http://proceedings.spiedigitallibrary.org/ on 08/24/2015 Terms of Use: http://spiedigitallibrary.org/ss/TermsOfUse.aspx

[92] T. V. Larson, G. S. Taylor, "On the evaporation of ammonium nitrate aerosol," Atmos. Environ. 17, 2605 (1983).
[93] M. C. Chang, C. Sioutas, S. Kim, H. Gong, W. S. Linn, "Reduction of nitrate losses from filter and impactor samplers by means of concentration enrichment," Atmospheric Environment 34, 85 (2000).
[94] D. Hu, J. Chen, X. Ye, L. Li, X. Yang, "Hygroscopicity and evaporation of ammonium chloride and ammonium nitrate: Relative humidity and size effects on the growth factor," Atmospheric Environment 45, 2349 (2011).
[95] K. Akiyama, Y. Morioka, I. Nakagawa, "Raman scattering and phase transition of Ammonium nitrates," Chem. Soc. Jap. 54, 1662 (1981).
[96] D. W. James, M. T. Carrick, W. H. Leong, "Structural Studies of Ammonium Nitrate - Phases III, IV, and V," Chem. Phys. Lett. 28, 117 (1974).
[97] W. M. Chien, D. Chandra, K. H. Lau, D. L. Hildenbrand, A. M. Helmy, "The vaporization of NH(4)NO(3)," J. Chem. Thermo. 42, 846 (2010).
[98] M. E. E. Harju, J. Valonen, "Effect of Sample Treatment on the phase transition paths of Ammonium Nitrate Solid State Phases IV, III, and II," J. Therm. Anal. 39, 681 (1993).
[99] Y. H. Cheng, C. J. Tsai, "Evaporation loss of ammonium nitrate particles during filter sampling," Journal of Aerosol Science 28, 1553 (1997).
[100] F. J. Owens, "Reproducible surface-enhanced Raman spectroscopy of small molecular anions," Mol. Phys. 109, 667 (2011).
[101] E. L. Holthoff, M. E. Hankus, P. M. Pellegrino, "Investigating a drop-on-demand microdispenser for standardized sample preparation," SPIE 8018:, F1 (2011).
[102] M. E. Hankus, D. N. Stratis-Cullum, P. M. Pellegrino, "Characterization of next-generation commercial surface-enhanced Raman scattering (SERS) substrates," SPIE 8018:, P1 (2011).
[103] T. V. Brook, in *USA TODAY*. (2013).

Downloaded From: http://proceedings.spiedigitallibrary.org/ on 08/24/2015 Terms of Use: http://spiedigitallibrary.org/ss/TermsOfUse.aspx

1	DEFENSE TECH INFO CTR
(PDF)	DTIC OCA
2	US ARMY RSRCH LAB
(PDF)	IMAL HRA MAIL & RECORDS MGMT
	TECHL LIB
1	GOVT PRNTG OFC
(PDF)	A MALHOTRA
4	US ARMY RSRCH LAB
(PDF)	ATTN RDRL SEE E
	M FARRELL
	E HOLTHOFF
	P PELLEGRINO
	G WOOD